

Superheavy nuclei with the vector self-coupling of the ω -meson in the relativistic mean-field theory

A A Saldanha, A R Farhan, M M Sharma

Physics Department, Kuwait University, Kuwait 13060, Kuwait

Abstract. We have studied properties and shell structure of the superheavy elements from $Z = 102$ to $Z = 120$ within the framework of the RMF theory. The region of study spans nuclides with neutron numbers $N = 150 - 190$. The Lagrangian model NL-SV1 with the inclusion of the vector self-coupling of the ω -meson has been employed in this work. We have performed RMF + BCS calculations for an axially deformed configuration of nuclei. The ground-state binding energies, single-particle properties and quadrupole deformation of nuclei have been obtained from the mean-field minimizations. Two-neutron separation energies, Q_α values and α -decay half-life have been evaluated. It is shown that a large number of nuclides exhibit the phenomenon of shape-coexistence over a significant region of the superheavy elements. Shape coexistence of a prolate and an oblate shape is prevalent in nuclides far below $N = 184$, whilst nuclei in the vicinity of $N = 184$ tend to show a shape coexistence between a spherical and an oblate shape. The shell structure and 2-neutron separation energies obtained with the RMF theory reinforce the neutron number $N = 184$ as a major magic number. It is shown that the neutron number $N = 172$ acts akin to a magic number in the deformed region. It is suggested that the combination $Z = 120$ and $N = 172$ has the potential of being a doubly magic number in the superheavy region.

PACS numbers: 21.10.-k, 21.10.Dr, 21.60.-n, 21.60.Jz, 27.90.+b

Submitted to: *J. Phys. G: Nucl. Phys.*

1. Introduction

Significant progress has been made in the discovery of new superheavy nuclei in the last decade [1, 2, 3, 4, 5, 6, 7, 8, 9, 10]. Superheavy elements at the extreme end of the periodic table have been synthesized in the laboratory. The synthesis of superheavy nuclei with $Z = 110 - 112$ at GSI, Darmstadt [3, 4] and JINR, Dubna [6, 7, 8, 9, 10] has stimulated the interest in the properties of superheavy nuclei. Discovery of isotopes of $Z = 112$ and $Z = 114$ was reported in JINR, Dubna and synthesis of $Z = 115$ at Berkeley was reported some time ago [10]. Earlier superheavy nuclei could be unambiguously identified by their α -decay chains leading to already known nuclei. However, the decay chains of the newly found superheavy nuclei cannot be linked to any nuclei known due to their relatively extreme positions in the periodic table. Therefore, their identification depends much upon a comparison with theoretical models.

Much progress has also been made in theoretical investigations of the properties of superheavy nuclei. Theoretical models such as macroscopic-microscopic (MM) models have been employed to discern and predict properties of superheavy nuclei. At the same time, various mean-field approaches have also been employed to investigate basic properties in this domain. The prediction of ${}_{184}^{298}114$ was confirmed by MM models such as FRDM with Folded Yukawa single-particle potential [11]. For the next doubly-magic nucleus, the available self-consistent models predict this to the more proton rich ${}_{172}^{292}120$ or the even heavier one at ${}_{184}^{310}126$. Predictions in various models tend to diverge primarily due differences in the form of the single-particle potentials.

Possibly different extrapolations arise in self-consistent Relativistic Mean-Field (RMF) theory. Here, the spin-orbit coupling is naturally built-in as a consequence of the Dirac-Lorentz structure of nucleons, whereas in all non-RMF models, it has to be introduced by hand. The non-RMF models tend to overestimate spin-orbit splitting with increase in mass number, thus affecting actual predictions of shell closures in the superheavy region. Superheavy nuclei with inherently large density of single-particle states can be a sensitive probe for models of nuclear structure.

Various microscopic approaches such as non-relativistic density-dependent Skyrme Hartree-Fock (SHF) theory [12, 13, 14, 15, 16, 17, 18] and that of MM type [19, 20, 21, 22, 23] are used extensively to investigate the properties and structure of superheavy nuclei. In the MM approach, a sum of smooth energy based upon liquid-drop type formula on which shell correction is imposed using the method of Strutinsky is obtained as the total binding energy of nuclei. The Finite-Range Droplet Model (FRDM) has achieved a significant success amongst the MM models. The mass formula FRDM is used to calculate the shell correction energies in order to identify the major magic numbers in the region of superheavy nuclei. A major proton magic number $Z = 114$ and a neutron magic number $N = 184$ have been predicted by the FRDM.

The MM approach has also been performed by Sobiczewski group [19, 20, 21, 22, 23], where the Strutinsky shell correction [24, 25] is used for the microscopic component, whereas Yukawa + exponential model is used for the macroscopic part. Superheavy

nuclei have also been studied extensively within the self-consistent mean-field models of Skyrme Hartree-Fock (SHF) type. Comparative studies of SHF and RMF models have been made. One of the first studies [26] performed within RMF theory earlier on was using the force NL-SH [27]. It was shown that neutron number $N = 184$ appears to be magic for lighter superheavy nuclei whereas its importance is reduced for heavier superheavies with $Z > 114$. There was also an indication of a small deformed shell-closure at $Z = 114$ for the proton number. In comparison, the FRDM predicted a strong shell gap at $Z = 114$ in the deformed region.

Extensive shell correction calculations were performed by Kruppa et al. [28] for sets of the Skyrme and RMF forces in order to identify the magic numbers in the region of superheavy elements theoretically. The Skyrme models predict the strongest shell effects for $N = 184$ and $Z = 124, 126$ and not at $Z = 114$, whereas RMF theory did not show a clear shell gap at $N = 184$ especially for heavier SHE. This was attributed to the difference in the shell structure in the above two approaches. This may have been due to a different isospin dependence in the Skyrme model as compared to the RMF theory [29, 30]. In comparison, all the Skyrme forces have predicted a broad valley of shell stabilization around $Z = 120$ and $N = 172$ and 184 . On the other hand, Cwiok *et al.* [31] have suggested a shift in the island of stability towards ${}_{184}^{310}126$.

In spite of an impressive agreement with experimental data for the heaviest elements, the theoretical uncertainties are large when extrapolating to unknown regions of the nuclear chart. In particular, there is no consensus among theories with regard to the regions of the shell stability for superheavy nuclei. Since in these nuclei the single-particle level density is relatively large, small shifts in the position of single-particle levels (e.g., due to the Coulomb or spin-orbit interaction) can be crucial for determining the shell stability of a nucleus. While most macroscopic-microscopic (non-self-consistent) models predict $Z = 114$ to be magic, most self-consistent calculations suggest that the center of the proton shell stability should be moved up to higher proton numbers, i.e., $Z = 120, 124$, or 126 . For neutrons most non-relativistic calculations predict magic gap at $N = 184$ while the relativistic mean-field theory yields $N = 172$ - due to a slightly different spin-orbit interaction [26]. The experimental determination of superheavy nuclei from this region will thus be very important for pinning down the fundamental question of the spin-orbit force.

A number of theoretical studies have been carried out within the framework of the RMF theory [37, 38, 39] to investigate properties of superheavy nuclei, in particular, α -decay properties. In ref. [38] the nature of possible magic numbers within the framework of spherical relativistic Hartree-Bogoliubov theory using various interactions has been studied. A recent theoretical work [17] sheds some light on the question of magic superheavy nuclei. According to the calculations, the patterns of single-particle levels are significantly modified in superheavy elements. Firstly, the overall level density grows with mass number A , as $\propto A^{1/3}$. Secondly, no pronounced and uniquely preferred energy gaps appear in the spectrum. This shows that shell closures which are to be associated with large gaps in the spectrum are not robust in superheavy nuclei. The

theory predicts that beyond $Z = 82$ and $N = 126$ the usual localization of shell effects at magic numbers is diminished. Instead, theory predicts fairly wide areas of large shell stabilization without magic gaps.

The Relativistic Mean-Field (RMF) theory [40] has proved to be successful as a framework for description of various facets of nuclear properties. In the RMF theory, the nuclear force is produced by a virtual exchange of various mesons. The nuclear saturation is achieved by a balance between an attractive σ - and a repulsive ω -field. The relativistic Lorentz covariance of the theory allows an intrinsic spin-orbit interaction based upon exchange of σ - and ω -mesons. This has been shown to be advantageous for properties which depend upon spin-orbit potential. An immediate advantage of the proper spin-orbit potential has been the success of the RMF theory to be able to describe the anomalous kink in the isotope shifts of Pb nuclei [41]. The isotopic shifts of Pb have been measured with a high precision using atomic beam laser spectroscopy and are known to show a pronounced kink about the magic number $N = 126$. The non-relativistic approaches based upon the Skyrme and Gogny forces have, on the other hand, been unable to reproduce this kink. It was shown that this difference in the predictions of the Skyrme model and the RMF theory is due to the isospin dependence of the spin-orbit term [29, 30]. The isospin dependence in the RMF theory is provided mainly by the coupling constant g_ρ of the ρ -meson. However, as the strength of the spin-orbit term derives from a large sum of the absolute values of the scalar and vector fields, the contribution of ρ -field is much weaker in comparison. Consequently, the isospin dependence of the spin-orbit potential in the RMF theory is relatively weak [29]. With the success of the RMF theory in properties of nuclei related to the shell effects, we have carried out a study of the superheavy nuclei with an RMF Lagrangian model which has been shown to have improved shell effects in nuclei.

In the present work, we have explored the region of superheavy nuclei within the framework of the relativistic mean-field theory using the Lagrangian model with the vector self-coupling of the ω meson. The region encompasses the superheavy elements from $Z = 102$ up to $Z = 120$. Nuclides in these isotopic chains with neutron number spanning $N = 150$ to $N = 190$ have been considered. We have used the force NL-SV1 due to Sharma et al. [34] with the vector self-coupling of the ω meson. Our focus is primarily to look for possible signatures of neutron shell gaps or magic numbers in the region of superheavy nuclei.

2. The Relativistic Mean-Field Theory: Formalism

In the present work, we have employed the RMF theory to study properties of superheavy nuclei. The starting point of the RMF theory is the model due to Walecka [40], which describes the nucleons as Dirac spinors interacting by the exchange of several mesons: scalar mesons (σ) couple to the nucleons (ψ) through a Yukawa term $\bar{\psi}\sigma\psi$ and produce strong attraction, isoscalar vector mesons (ω) couple to the conserved nucleon current $\bar{\psi}\gamma_\mu\psi$ and cause almost as strong a repulsion. In addition, there are isovector

ρ mesons which couple to the isovector current and photons to produce the well-known electromagnetic interaction.

We restrict ourselves to the Hartree treatment, where the A independent nucleons with the single-particle spinors ψ_i ($i= 1, \dots, A$) form a Slater determinant and move independently in the meson fields. The RMF theory starts with the standard Lagrangian density

$$\begin{aligned}
 \mathcal{L} = & \bar{\psi}_i \{ i\gamma^\mu \partial_\mu - M \} \psi_i \\
 & + \frac{1}{2} \partial^\mu \sigma \partial_\mu \sigma - U(\sigma) - g_\sigma \bar{\psi}_i \sigma \psi_i \\
 & - \frac{1}{4} \Omega^{\mu\nu} \Omega_{\mu\nu} + \frac{1}{2} m_\omega^2 \omega^\mu \omega_\mu - g_\omega \bar{\psi}_i \gamma^\mu \omega_\mu \psi_i \\
 & - \frac{1}{4} \vec{R}^{\mu\nu} \vec{R}_{\mu\nu} + \frac{1}{2} m_\rho^2 \vec{\rho}^\mu \vec{\rho}_\mu - g_\rho \bar{\psi}_i \gamma^\mu \vec{\rho}_\mu \vec{\tau} \psi_i \\
 & - \frac{1}{4} F^{\mu\nu} F_{\mu\nu} - e \bar{\psi}_i \gamma^\mu A_\mu \frac{(1 - \tau_3)}{2} \psi_i \\
 & + \frac{1}{4} g_4 (\omega_\mu \omega^\mu)^2,
 \end{aligned} \tag{1}$$

where the summation convention is used and the sum over i runs over all nucleons. Isovector quantities are indicated by the arrow bars. As proposed by Boguta and Bodmer [42], the σ meson moves in a nonlinear potential of the form:

$$U(\sigma) = \frac{1}{2} m_\sigma \sigma^2 + \frac{1}{3} g_2 \sigma^3 + \frac{1}{4} g_3 \sigma^4. \tag{2}$$

Here, M , m_σ , m_ω and m_ρ are the nucleon, the σ -, the ω -, and the ρ - meson masses, respectively. g_σ , g_ω , g_ρ , and $e^2/4\pi=1/137$ are the coupling constants for the σ -, the ω -, the ρ -mesons and for the photon. The coupling constant g_4 represents the vector self-coupling of ω -meson as introduced in ref. [34].

The classical variation principle provides the Klein-Gordon equations for the mesons:

$$\begin{aligned}
 \{-\Delta + m_\sigma^2\} \sigma(\mathbf{r}) &= -g_\sigma \rho_s(\mathbf{r}) - g_2 \sigma^2(\mathbf{r}) - g_3 \sigma^3(\mathbf{r}) \\
 \{-\Delta + m_\omega^2\} \omega^\mu(\mathbf{r}) &= g_\omega j^\mu(\mathbf{r}) + g_4 \omega^3(\mathbf{r}) \\
 \{-\Delta + m_\rho^2\} \vec{\rho}^\mu(\mathbf{r}) &= g_\rho j^\mu(\mathbf{r}) \\
 -\Delta A^\mu(\mathbf{r}) &= e j_p^\mu(\mathbf{r}),
 \end{aligned} \tag{3}$$

whereby the sources are determined by the corresponding density and current distributions in the static nucleus. Variation for the nucleonic field gives the Dirac equation for nucleons:

$$\{-i\alpha \cdot \nabla + \beta M^*(r) + V(r)\} \psi_i(r) = \epsilon_i \psi_i(r). \tag{4}$$

The effective mass $M^*(r)$ is determined by the scalar field $\sigma(r)$ as

$$M^*(r) = M + g_\sigma \sigma(r), \tag{5}$$

and the potential vector potential $V(\mathbf{r})$ is obtained as:

$$V(\mathbf{r}) = g_\omega \omega_0(\mathbf{r}) + g_\rho \tau_3 \rho_0(\mathbf{r}) + e \frac{(1 - \tau_3)}{2} A_0(\mathbf{r}). \quad (6)$$

Bold faced letters indicate vectors in the 3-dimensional space. These fields are the solutions of the inhomogeneous Klein-Gordon equations. As is the case in the majority of applications, the contributions of antiparticles are neglected, i.e., the *no-sea* approximation is employed. Equation (3) together with Eq. (4) provides a closed set of equations. In order to describe the ground-state properties of nuclei, static solutions are obtained from the equations of motion Eqs. (3-4). In this case, the nucleon spinors are the eigenvectors of the stationary Dirac equation, which yields the single-particle energies ϵ_i as eigenvalues. The solution of these equations is obtained iteratively. Using these solutions, one calculates physical quantities such as the total energy, charge radii and quadrupole moments among others.

2.1. Axially deformed RMF

For nuclei in the superheavy region exhibit significant deformations, we have employed the RMF theory for axially deformed configuration of nuclei. We solve the Dirac equation (3) as well as the Klein-Gordon equations (4) by expansion of the wavefunctions into a complete set of eigen solutions of an harmonic oscillator potential [43]. In the axially symmetric case the spinors f_i^\pm and g_i^\pm are expanded in terms of the eigenfunctions of a deformed axially symmetric oscillator potential

$$V_{osc}(z, r_\perp) = \frac{1}{2} M \omega_z^2 z^2 + \frac{1}{2} M \omega_\perp^2 r_\perp^2. \quad (7)$$

Taking volume conservation into account, the two oscillator frequencies $\hbar\omega_\perp$ and $\hbar\omega_z$ can be expressed in terms of a deformation parameter β_0 .

$$\hbar\omega_z = \hbar\omega_0 \exp\left(-\sqrt{\frac{5}{4\pi}}\beta_0\right) \quad (8)$$

$$\hbar\omega_\perp = \hbar\omega_0 \exp\left(+\frac{1}{2}\sqrt{\frac{5}{4\pi}}\beta_0\right). \quad (9)$$

The corresponding oscillator length parameters are given by

$$b_z = \sqrt{\frac{\hbar}{M\omega_z}} \quad \text{and} \quad b_\perp = \sqrt{\frac{\hbar}{M\omega_\perp}}. \quad (10)$$

The volume conservation gives $b_\perp^2 b_z = b_0^3$. The basis is now determined by the two constants $\hbar\omega_0$ and β_0 , which are chosen optimally.

The deformation parameter of the oscillator basis β_0 is chosen to be identical for the Dirac spinors and the meson fields. The deformation parameter β_2 is obtained from the calculated quadrupole moments for protons and neutrons through

$$Q = Q_n + Q_p = \sqrt{\frac{16\pi}{5}} \frac{3}{4\pi} A R_0^2 \beta_2 \quad (11)$$

with $R_0 = 1.2A^{1/3}$ (fm). The quadrupole moments are calculated by using the expression:

$$Q_{n,p} = \langle 2r^2 P_2(\cos\theta) \rangle_{n,p} = 2\langle 2z^2 - x^2 - y^2 \rangle_{n,p}. \quad (12)$$

2.2. Shell effect in nuclei

Shell effects play an important role in identifying and consequently synthesizing superheavy elements due to additional stability provided by the shell effects. Hence few comments on shell effects would be in order. The shell effects manifest strongly in nuclei with the existence of magic numbers. The origin of shell closure has long been understood due to spin-orbit coupling and to an ensuing splitting of levels. The spin-orbit potential and a bunching of levels create shell closures (magic numbers) which are predicted correctly by most of the models. In the non-relativistic density-dependent theory of the Skyrme type, the spin-orbit interaction is added phenomenologically and its strength is adjusted to reproduce the spin-orbit splitting in ^{16}O . In the RMF theory, on the other hand, the spin-orbit interaction arises naturally due to exchange of σ and ω mesons between the nucleons. The strength of the interaction is determined by the spin-orbit splitting in ^{16}O and other nuclei, which is uniquely decided by the effective mass. As mentioned in the introduction, the shell effects in the RMF theory have been advantageous in a few aspects such as isotope shifts in nuclei. In view of this, application of the RMF theory to superheavy nuclei may have more realistic predictions.

2.3. Lagrangian with the vector self-coupling of ω -meson

In this work, we have employed the Lagrangian model with the quartic coupling of ω meson. The non-linear vector self-coupling of ω -meson was introduced by Bodmer [44] and properties of nuclear matter were discussed on adding a quartic term in ω -meson potential. The inclusion of the vector self-coupling of ω meson in addition to the non-linear scalar self-coupling of σ meson was found to have the effect of softening the high-density equation of state (EOS) of the nuclear matter [45]. Subsequently, the force NL-SV1 [34] with the inclusion of the vector self-coupling of ω meson was developed with a view to improve the predictions of the ground-state properties of nuclei, such as binding energies, charge radii and isotopes shifts of nuclei along the stability line. It was shown that with the Lagrangian model NL-SV1, the shell gaps in nuclei along the stability line such as Ni and Sn isotopic chains were improved as compared to Lagrangian model with the nonlinear scalar coupling alone [34]. With the improved shell structure along the line of β -stability with NL-SV1, it is expected that it shall have improved predictions in the region far away from the stability line. In view of this, we have used the parameter set NL-SV1 with the vector self-coupling of ω meson in our investigations. The parameters of the parameter set NL-SV1 [34] are given in Table I.

Table 1. The Lagrangian parameters of the force NL-SV1 [34] used in the RMF calculations.

Parameters	NL-SV1
M	939.0
m_σ	510.0349
m_ω	783.0
m_ρ	763.0
g_σ	10.1248
g_ω	12.7266
g_ρ	4.4920
g_2	-9.2406
g_3	-15.388
g_4	41.0102

3. Details of calculations

The input parameters required to carry out explicit numerical calculations are: neutron pairing gap Δ_n , the proton pairing gap Δ_p and the number of oscillator shells N_F and N_B of the fermionic wavefunctions and meson fields, respectively. Both the fermionic and bosonic wavefunctions have been expanded in a basis of 20 harmonic oscillator shells in this work.

We have carried out a study of superheavy nuclei from No ($Z = 102$) to $Z = 120$. The neutron number ranges from $N = 150$ to $N = 190$. This region encompasses the neutron number $N = 184$ which has been predicted to be a magic number in various theories. A possible deformed shell has also been predicted in this region as discussed in Section I. We have carried out deformed RMF+BCS calculations for superheavy nuclei in the above region. For pairing gaps, we have used the formula due to Möller and Nix [46] as given by:

$$\Delta_n = 4.8 N^{-1/3} \tag{13}$$

$$\Delta_p = 4.8 Z^{-1/3}. \tag{14}$$

An axially symmetric deformed configuration with reflection symmetry has been assumed for nuclei. For each nucleus an initial basis deformation of prolate as well as oblate type has been taken in order to seek a minimum both in the prolate as well as in the oblate region of the deformation space. Consequently, we have obtained a prolate and an oblate minimum for most of the nuclei. However, nuclei close to a potential magic number assume a spherical shape.

4. Results and Discussions

4.1. Binding energies and deformations

The RMF+BCS minimizations with NL-SV1 give rise to a prolate and an oblate solution for most of the nuclei. We show the quadrupole deformation β_2 for the lowest energy state (ground state) for all the isotopic chains in Figures 1(a)- 1(j). A large number of nuclei in these chains assume a prolate shape in the ground state. This is especially the case in the region of neutron number $N \sim 150 - 170$. Typically, these nuclei exhibit a prolate deformation of $\beta_2 \sim 0.2 - 0.3$.

For the isotopic chains of No ($Z = 102$), Rf ($Z = 104$) and Sg ($Z = 106$), there is a transition from a prolate shape to an oblate shape at $N \sim 170$. Beyond $N = 172$, nuclei assume an oblate shape in the ground state for these isotopic chains (see Figs. 1(a)– 1(d)). The magnitude of the oblate deformation decreases as the neutron number increases above $N = 172$, which approaches a vanishing value as the neutron number $N = 184$ arrives. In the vicinity of $N = 184$, nuclei exhibit a spherical shape. Such a feature has been commonly predicted by several relativistic as well as non-relativistic theories, whereby $N = 184$ constitutes a major magic number in the region of superheavy nuclei.

As one goes to the heavier elements above Sg ($Z = 106$), one can visualize that the tendency of prolate shapes in the range of neutron numbers $N = 150 - 176$ continues for heavier superheavy elements as well. The point of shape transition from prolate to oblate seems to be shifting to a higher neutron number. For instance, for Hs ($Z = 108$) the prolate to oblate transition occurs at $N = 178$. For the isotopic chain Ds ($Z = 110$) the shape transition point advances to $N = 180$. However, for $Z = 112$ and above, the transition point falls back to $N = 178$ and below it. For instance, for $Z = 116$ and $Z = 118$, the shape transition occurs at $N = 174$ and $N = 172$, respectively. Similarly, the shape transition point for $Z = 120$ falls back to $N = 170$. Thus, the number of nuclei which exhibit an oblate shape below the neutron number $N = 184$ increases steadily in going from $Z = 112$ to $Z = 120$. As far as the spherical shape for $N = 184$ nuclei is concerned, it is exhibited by all the isotopic chains from $Z = 102$ to $Z = 120$. This is reminiscent of a magic shell character for the neutron number 184.

The general feature of shape transition from prolate to oblate in the region of $N = 172 - 176$ prevails for all the isotopic chains considered in this study. We have made a comparison of NL-SV1 deformations with those predicted by the macroscopic-microscopic mass formula FRDM. For the isotopic chains $Z = 102 - 112$, the FRDM exhibits a predominantly prolate shape for the neutron numbers $N = 150 - 176$. This feature is very similar to that predicted by NL-SV1.

The FRDM shows a shape transition from prolate to an oblate shape at the neutron number $N \sim 178$ for the chains $Z = 102 - 110$. There is only a single nuclide exhibiting an oblate shape in FRDM at $N \sim 178$ for these chains, beyond which all the nuclei assume a spherical shape for the isotopic chains of $Z = 102 - 112$ in the FRDM predictions, in contrast to NL-SV1. The oblate deformation for $N = 178$ nuclei in this

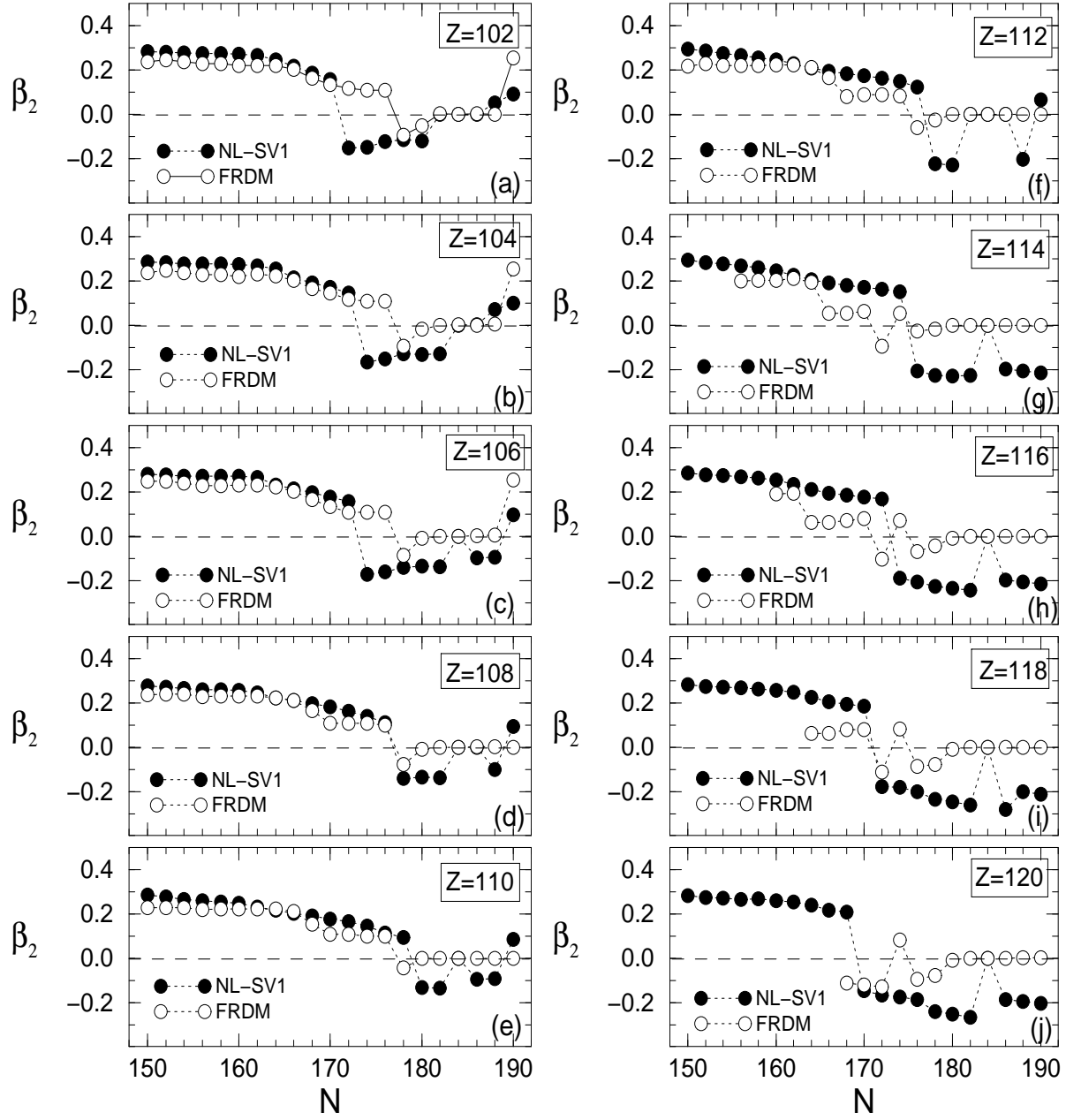


Figure 1. The β_2 values for isotopes of the elements $Z = 102 - 120$ obtained with NL-SV1. The results with FRDM are shown for comparison.

region amounts to $\beta_2 \sim 0.1$ in the FRDM. This is unlike NL-SV1, where a significant number of nuclei exhibit a moderately deformed oblate shape until the supposedly magic number $N = 184$ arrived at.

For the isotopic chains $Z = 114 - 118$, the behaviour of FRDM for deformation properties is rather uneven. For the region of the lower neutron numbers, some nuclei in these chains show a moderately prolate shape, whereas a few others exhibit a small prolate deformation. This is followed by a shape transition to an oblate deformation

at $N = 172$, followed by a spherical shape in going to higher neutron numbers. That nuclei in the vicinity of $N = 184$ are predominantly spherical in FRDM points to the hypothesis that $N = 184$ maintains its magicity even for heavier superheavy elements in FRDM.

4.2. Comparison with ETF-SI results

The mass formula Extended Thomas-Fermi with Strutinsky integral (ETF-SI) [47] was obtained to fit experimental masses of more than 1600 nuclei from all over the periodic table. The ETF-SI, due to its partly microscopic structure, has found broader acceptance for nuclear physics applications. It predicts binding energies and deformations of nuclei over a broad range of masses quite well. Here we compare the ground state deformations obtained with NL-SV1 with those predicted by ETF-SI. The quadrupole deformations β_2 are compared for the given isotopic chains in Figs. 2(a)–2(j). Figs. 2(a)–2(d) show that ETF-SI deformations are in good agreement with the NL-SV1 values from $N = 150$ to $N \sim 166$ for the elements from Ds ($Z = 102$) to Hs ($Z = 108$). For Ds ($Z = 110$), the agreement between NL-SV1 and ETF-SI is good up to $N = 164$ (see Fig. 2(e)).

A contrasting picture with the ETF-SI is that for neutron numbers $N \sim 166$ and above, it shows a strong divergence from the NL-SV1 predictions. ETF-SI does not exhibit a prolate to oblate transition as do NL-SV1 and FRDM predictions. In contrast, ETF-SI predicts a constant and a large value of $\beta_2 \sim 0.4$ for nuclei in the range of $N \sim 168 - 180$ for the isotopic chains of $Z = 102 - 110$. For the heavier elements $Z = 112 - 120$, ETF-SI predicts a nearly constant value $\beta_2 \sim 0.4$ for all the neutron numbers $N = 150 - 180$.

ETF-SI predicts a spherical shape of nuclei in the vicinity of $N = 184$ for the elements $Z = 102 - 114$. This feature of ETF-SI is similar to that of FRDM. However, for $Z = 116$, ETF-SI bypasses the spherical shape for $N = 184$. On the other hand, for several isotopic chains ETF-SI predicts a shape transition from spherical to a strongly prolate shape at $N = 188 - 190$ (see Figs. 2(b)– 2(g)).

For $Z = 110$ and $Z = 112$, nuclei with two neutrons below and two neutrons above $N = 184$ exhibit a spherical shape, whereas for $Z = 114$ there is only one nuclide i.e., $N = 184$ that shows a spherical shape. Its neighbours on both sides, assume a prolate shape in ETF-SI. This is indicative of a decrease in the shell strength at $N = 184$ with ETF-SI. This point is supported by a deformed shape taken by the $N = 184$ nuclide for $Z = 116$ (See Fig. 2(h).) with ETF-SI. Whilst ETF-SI values for $Z = 118$ and $Z = 120$ are not known, the aforesaid diminishing of $N = 184$ shell strength points to an erosion of a possible $N = 184$ magicity for the heaviest superheavy elements from $Z = 116$ to $Z = 120$ with ETF-SI.

A summary of quadrupole deformation β_2 in the ground state of superheavy nuclei with NL-SV1 obtained in this work is shown in the Fig 3. The nuclei denoted by the red colour indicate a prolate ground state. An oblate ground state is shown by the

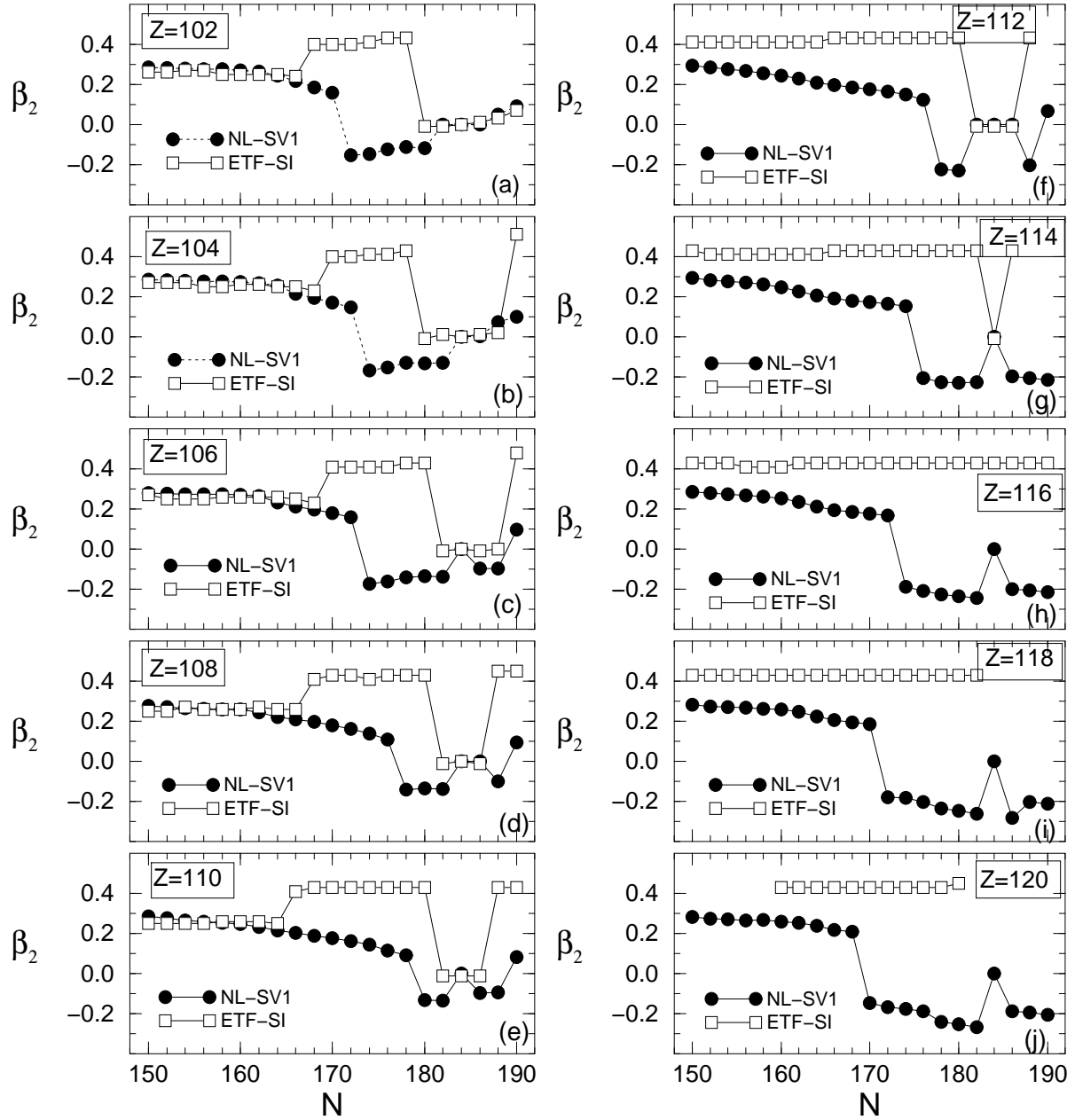


Figure 2. The β_2 values for the isotopes of the elements $Z = 102 - 120$ obtained with NL-SV1 are compared with ETF-SI predictions.

green colour. Spherical nuclei are indicated by yellow. As seen in Fig. 3, nuclides with $N = 150 - 172$ for almost all the isotopic chains exhibit a prolate shape. On the other hand, nuclides with $N > 172$ exhibit an oblate shape until a spherical shape appears for nuclei close to $N = 184$. There is a little exception here in that for SHE with $Z = 108$ to $Z = 112$, a few nuclides above $N = 172$ continue to exhibit a prolate shape. This indicates an intrusion of prolate shape into the domain of oblate shapes as indicated in the middle of the figure. Nuclei in the vicinity of $N = 184$ are predominantly spherical

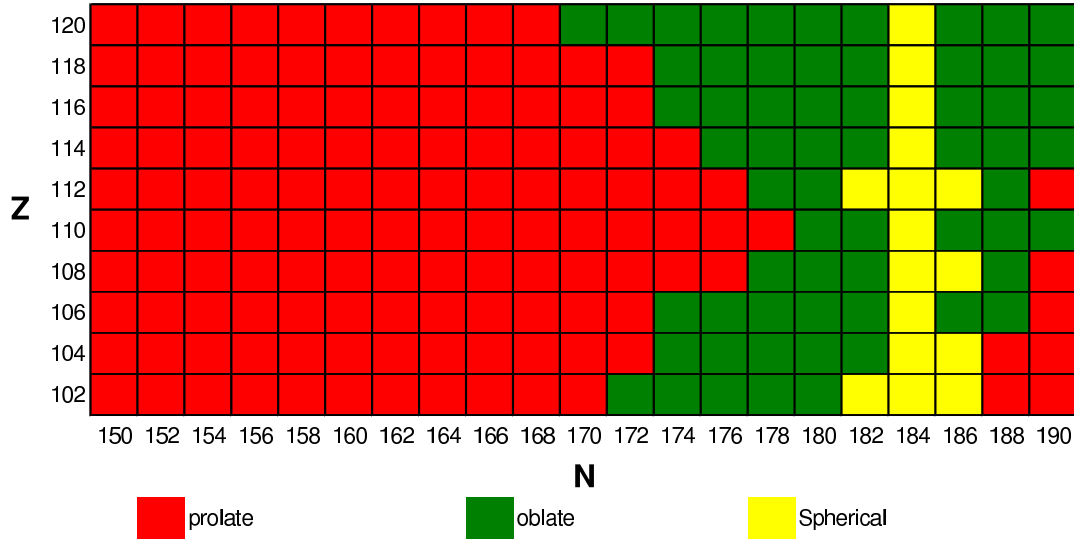


Figure 3. The landscape of the quadrupole deformation β_2 obtained with NL-SV1 for $Z = 102 - 120$ and $N = 150 - 190$.

as shown by the yellow blocks. In a few cases and especially for $Z = 102$, nuclei two neutrons below and two neutrons above $N = 184$ assume a spherical shape. As shown by the picture, $N = 184$ acts as a major magic number in the neutron-rich region for all the SHE with $Z = 102 - 120$.

As we will see in the single-particle levels, the neutron number $N = 184$ remains as a major magic number. Also we will see that in the RMF theory with NL-SV1, the proton number $Z = 120$ is also a magic number. The combination $Z = 120$ and $N = 184$ seems to act as double closed shell in the RMF theory.

Nuclides above $N = 184$ show a prolate (red) region for a few lighter SHE. However, for heavy SHE with $Z = 108$, nuclides above $N = 184$ are predominantly oblate (green) as shown in the Fig. 3. Thus, a significant region below as well as above $N = 184$ lends itself to an oblate deformation.

4.3. Shape co-existence in the superheavy region

The phenomenon of shape co-existence in the region of deformed nuclei arises due to interplay of deformed single-particle levels. Splittings and alignment of deformed single-particle levels leads often to ground states with a prolate and an oblate shape nearly degenerate in energy. For practical purposes, when the two minimum energy states are within ~ 1 MeV, the two states are said to be shape co-existent.

We show in Figs. 4(a)–4(j) nuclides which exhibit a shape co-existence with NL-SV1. Looking at the figures one can see that a large number of nuclides exhibit the shape co-existence for the superheavy chains. The nuclides in isotopic chains from $Z = 102$ (No) to $Z = 112$ show a common pattern of shape co-existence between prolate and

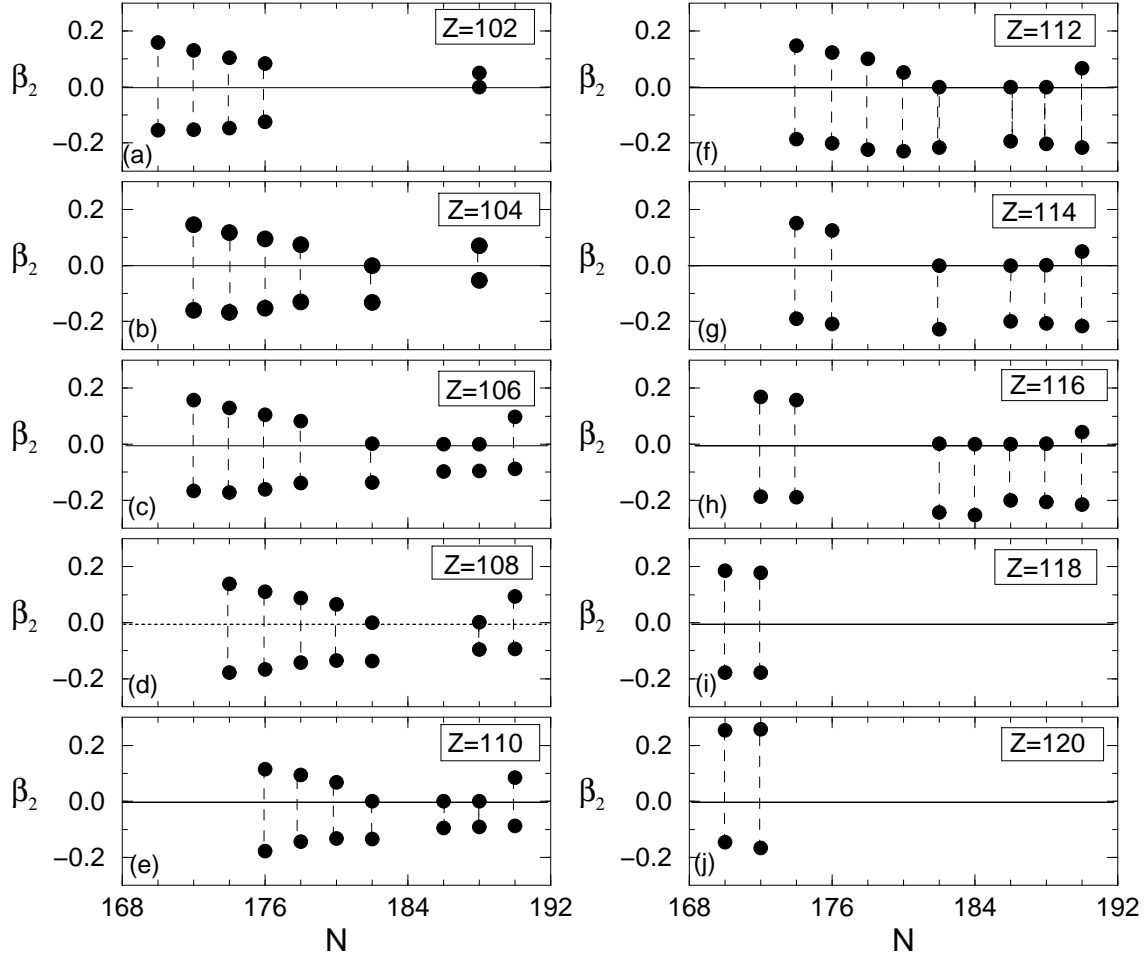


Figure 4. Isotopes of $Z = 102$ – 120 exhibiting the shape-coexistence in the Lagrangian model NL-SV1.

oblate shapes for the region of neutron numbers $N \sim 170$ to $N \sim 182$. Whilst for $Z = 102$ and $Z = 104$ shape co-existence is limited to neutron numbers $N \sim 168$ to $N \sim 178$, for $Z = 106$ to $Z = 112$ the region of shape co-existence extends to neutron number $N = 182$. Whereas for the lighter neutron numbers there is a prolate-oblate shape co-existence for elements $Z = 102$ to $Z = 112$, there is a shape co-existence of spherical-oblate shapes for $N = 182$ isotones from $Z = 104$ – 112 . This indicates a softer nature of $N = 184$ shell closure even for the lighter superheavy elements. Several nuclides with $N > 184$, also exhibit a spherical-oblate shape co-existence for the isotopic chains $Z = 106$ – 112 .

Figures 4(g)- 4(j) show the shape co-existence for heavier superheavy elements from $Z = 114$ to $Z = 120$. Unlike the picture for superheavy elements $Z = 102$ – 112 , the shape co-existence in the lighter neutron region is reduced significantly for $Z = 114$ – 120 . Only a few nuclides below $N = 180$ exhibit a prolate-oblate shape co-existence. For $Z = 114$ and $Z = 116$, several nuclides exhibit a spherical-oblate shape co-existence

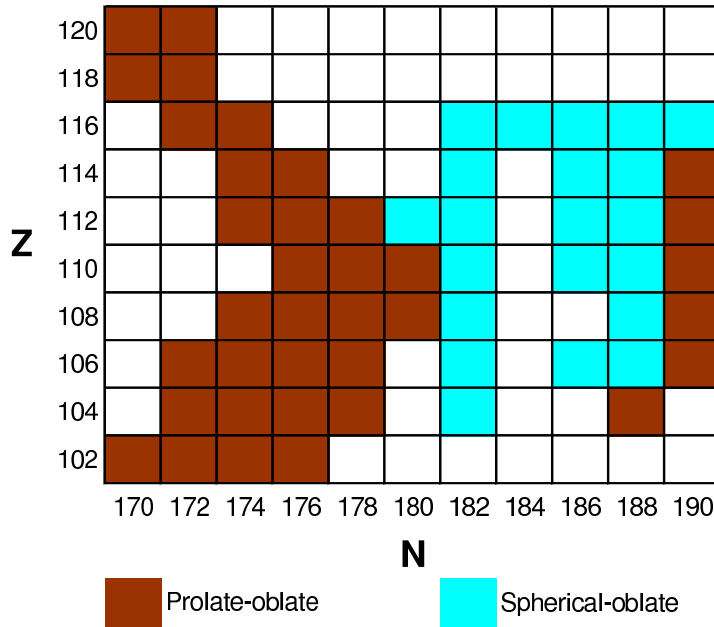


Figure 5. The landscape of shape co-existence in superheavy nuclei with NL-SV1. The prolate-oblate and spherical-oblate shape co-existence is depicted.

for neutron numbers $N > 184$. Interestingly, $N = 184$ nuclide for $Z = 116$ shows a spherical-oblate shape co-existence. This indicates a softening of the shell effects for $N = 184$ for $Z = 116$.

The superheavy elements $Z = 118$ and $Z = 120$ exhibit the shape co-existence rather scarcely i.e, only two isotopes $N = 170$ and $N = 172$ show a prolate-oblate shape co-existence. In the rest of the neutron region, there is no shape co-existence for the heaviest superheavy elements with $Z = 118$ and $Z = 120$. This may imply that the shell strength at $N = 184$ has picked up for these chains and that a readjustment of the deformed single-particle levels does not lend to degenerate shapes in the ground state.

A summary of the shape co-existence in superheavy nuclei is illustrated in Fig. 5. The brown squares depict a shape co-existence between a prolate and an oblate shape, whereas the blue squares represent a shape co-existence between a spherical and an oblate shape. As the figure shows, the phenomenon of prolate-oblate shape co-existence pervades the region from $N = 170$ to $N = 180$. For the lighter elements this shape co-existence lies in the neutron region 170-178. The lower boundary of this region gradually shifts to higher neutron numbers $Z = 110$ is reached. As one moves above $Z = 110$, the region shifts gradually towards lower neutron numbers again. From $Z = 114$ to $Z = 120$, however, there are fewer cases of the prolate-oblate shape co-existence. Apparently, the region of prolate-oblate shape co-existence as shown by the brown colour is symmetric about $Z = 110$. In addition, there are a few more cases of prolate-oblate shape co-existence for higher neutron numbers near $N = 190$.

The region of spherical-oblate shape co-existence lies near $N = 184$. The neutron

number $N = 184$ being a major magic number, the ground-state of nuclides with $N = 184$ is spherical as seen earlier. For almost all the isotopic chains there is no shape co-existence (empty squares) at $N = 184$, with the exception of $Z = 116$. Only for $Z = 116$, there is a spherical-oblate shape co-existence at $N = 184$. This is due to an erosion of the magicity of $N = 184$ for $Z = 116$.

Nuclides with $N = 182$ show a spherical-oblate shape co-existence as shown by blue squares. Nuclides with $N = 186$ and $N = 188$ also exhibit a spherical-oblate shape co-existence for several isotopic chains. The fact that nuclides just below and above $N = 184$ display a spherical shape co-existence indicates that $N = 184$ is not such a strong magic number. This can be contrasted with other magic numbers in the periodic table which exhibit robustness. There are rarely occasions of a shape-coexistence or even a deformation in the direct vicinity of a major magic number especially when one is not very far from the line of β -stability. Superheavy nuclei especially those associated to $N = 184$ do not fall in this category and are deemed to be in a region far from the stability line. Therefore, mellowing of the shell strength of $N = 184$ is not unexpected.

4.4. Two-neutron separation energies

Magic numbers in nuclei are characterized by a large shell gap between the last single-particle level of the magic number and the next single-particle level above it. This results in a larger value of 2-neutron separation energy S_{2n} for a nucleus with 2-neutrons more than the magic number. Consequently, the major magic numbers exhibit a characteristic kink in S_{2n} values all over the periodic table. Thus, the difference $S_{2n}(N) - S_{2n}(N + 2)$ at the magic neutron number N reflects its shell gap. Its magnitude is a measure of the shell strength.

With a view to visualize as to whether there are possible shell closures in neutron numbers for superheavy nuclei, we have computed S_{2n} values for all the isotopic chains. Using the binding energies of neighbouring isotopes, S_{2n} is defined as,

$$S_{2n} = B.E. (N) - B.E (N + 2). \quad (15)$$

The S_{2n} values for the isotopic chains considered in this work are shown in Fig. 6. The values correspond to the lowest energy state (ground state) obtained with RMF+BCS minimization using the force NL-SV1. As expected, the S_{2n} values show a decreasing trend in going to nuclei with higher neutrons. The S_{2n} values show a rather monotonous decrease in going from $N = 152$ to $N \sim 170$ with a slight kink-like structure in the neighbourhood of $N \sim 154$ and $N \sim 164$. Due to significant changes in deformation properties of nuclei near $N \sim 172$ and $N \sim 184$, there is much more structure in the S_{2n} values.

In order to visualize the structure in the S_{2n} values, we have split Fig. 16 into two parts which are shown in Fig. 7. In Fig. 17 (a) the S_{2n} values for $N = 152 - 168$ are shown. The higher neutron part with $N = 168 - 190$ is shown in Fig. 7 (b). One can notice a slight kink at $N = 154$ for several isotopic chains. A kink like structure is visible for $Z = 106 - 116$. This structure diminishes for $Z = 118$ and $Z = 120$.

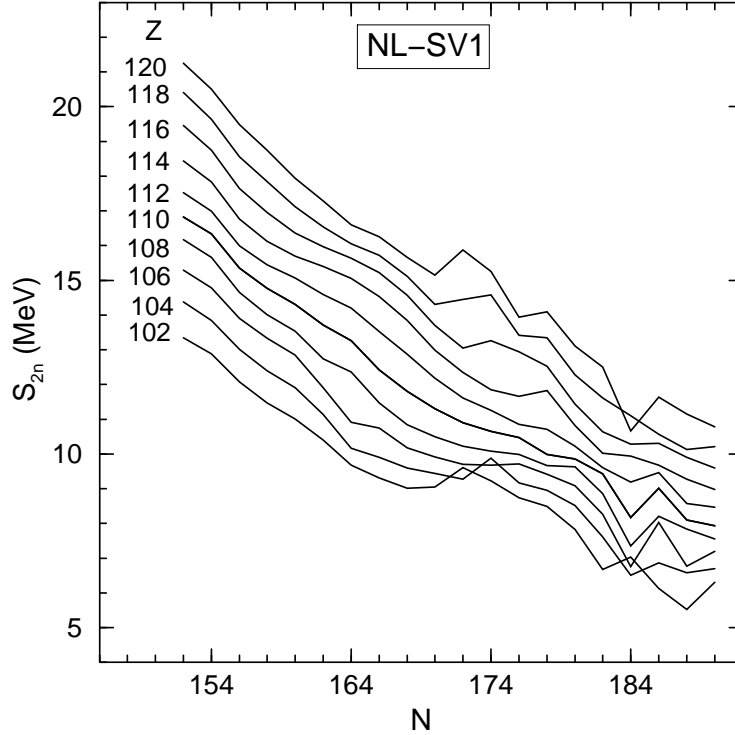


Figure 6. Two-neutron separation energy S_{2n} for the isotopes of $Z = 102$ to $Z = 120$ with neutron numbers ranging from $N = 150$ to $N = 190$.

The structure at $N = 154$ is compatible with a deformed shell gap predicted by non-relativistic macroscopic-microscopic approaches [13].

One can also notice a slight kink at $N \sim 164$. Thus, there seems to exist a few pockets of presumably deformed shell gaps at $N \sim 154$ and $N \sim 164$. However, there are no signatures of any strong magic number in the region $N = 152 - 168$. Fig. 7 (b) shows structures in S_{2n} values at $N \sim 172$, 178 and 184. The behaviour of S_{2n} values in the neutron region $N = 168 - 190$ is far from monotonous. However, for the lighter superheavy elements, there is very little structure at $N \sim 172$ except for $Z = 102$ and 104. For the heavier elements with $Z = 116 - 120$, the kink at $N \sim 172$ shows a slightly upward trend. A kink like structure in this region indicates a possible $N \sim 172$ deformed shell gap for superheavy elements. A combination of $N \sim 172$ and $Z \sim 120$ might lend itself to a structure akin to a double shell closure.

The region near $N \sim 184$ is full of structural effects as can be seen in Fig. 7 (b). A kink in the S_{2n} values can be seen clearly at $N = 184$ in several isotopic chains with $Z = 104 - 110$. Thus, for the lighter superheavy elements NL-SV1 predicts a shell closure at $N = 184$ as indicated by the kink. For the deformed RMF+BCS calculations with NL-SV1, a sharp decrease in the S_{2n} values at $N = 184$ is indicative of a shell closure which is consistent with that with NL-SH [26]. For SHE above $Z \geq 112$ the kink and the structure at $N = 184$ is reduced significantly. Thus, for the heaviest SHE, S_{2n} values do not give an unambiguous indication of a shell closure at $N = 184$.

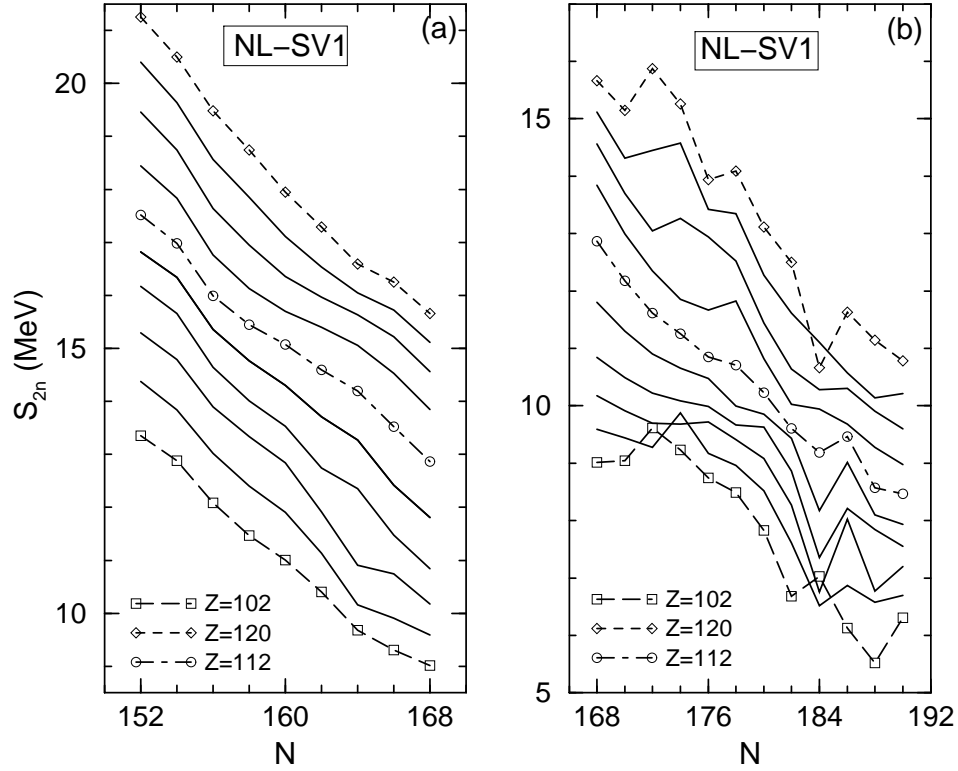


Figure 7. (a) Two-neutron separation energy S_{2n} for the isotopes of elements $Z = 102$ to $Z = 120$, with neutron numbers ranging from $N = 152$ to $N = 170$. (b) S_{2n} values for $N = 170$ to $N = 190$.

4.5. Alpha-decay properties - Q_α values

In the pursuit of superheavy heavy elements, it is one of aims of research to find out regions of extra-stability with a view to synthesize superheavy elements with the most appropriate projectile and target combinations. With this in mind, it will be helpful if one can explore the regions of higher stability theoretically. Depending upon the region of an extra-stability which would arise from shell gaps and possible shell closures, the half-life of α -decay is a potential indicator of a possible value of stability for an area of enhanced stability. It is expected that for nuclei near a shell closure the α -decay half-lives would be larger than their neighbours.

Nuclei in the transuranium and superheavy region are known to be α emitters. The rate of α -decay depends strongly on Q_α value of a nucleus. We have calculated Q_α values for nuclei in all the isotopic chains we have considered. The Q_α values thus obtained are shown in Fig. 8. As one moves from $Z = 104$ to $Z = 120$, Q_α values show a continuous increase with increase in the charge number of a nucleus. For all the isotopic chains one can see a decrease in the Q_α values with an increase in neutron number. A decreasing α -value implies a higher α -decay half-life. Consequently, in moving from the lower neutron number $N = 150$ towards $N = 184$, one has a stabilizing factor with a decrease in the Q_α values. For nuclides with $N = 186$, a slight peak in Q_α -values for

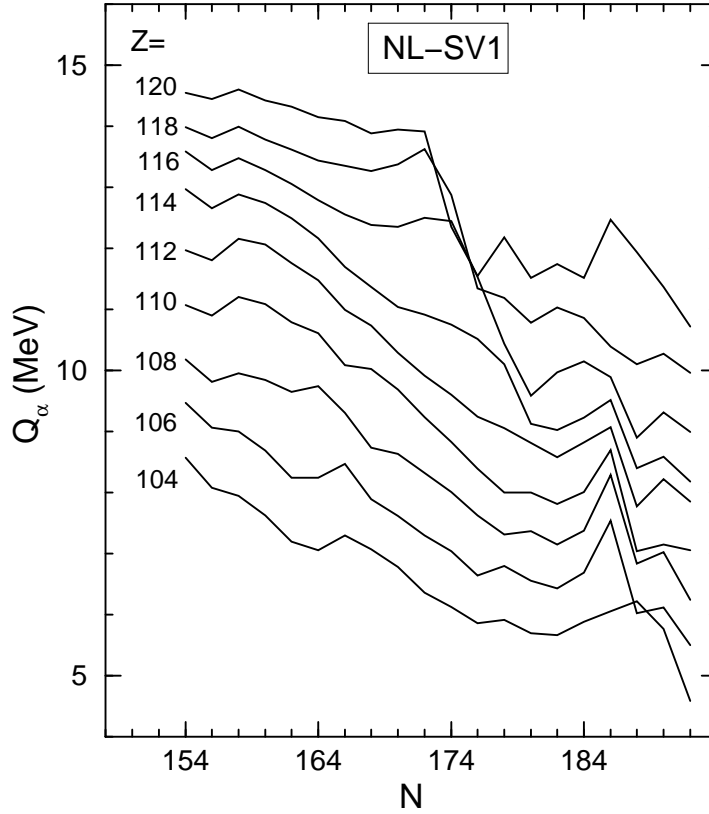


Figure 8. Q_α values for the isotopic chains with $Z = 102 - 120$ and $N = 150 - 190$ obtained with NL-SV1.

several isotopic chains with $Z = 104 - 114$ can be seen. In terms of α -decay half-life (as we will see below) it will mean that nuclides with $N = 186$ become more unstable towards α -decay.

In going above $N = 184$ one sees a little peak at $N = 186$ for the isotopic chains with $Z = 106 - 114$, though for the chain with $Z = 104$, Q_α shows an increasing trend from $N = 184$ to $N = 186$. In terms of α -decay half-life this would imply a decreased half-life for nuclides with $N = 186$. For the isotopic chains above $Z = 114$ such a behaviour is not seen, but for only $Z = 120$. Above $N = 186$, there is a decrease in Q_α values for all the isotopic chains.

4.6. Comparison with the experimental data (systematics)

A large amount of experimental effort to the synthesis of superheavy elements as well as to explore the nuclear properties of superheavy nuclei by the Lawrence Berkeley National Laboratory, Berkeley, GSI, Darmstadt and the Joint Institute for Nuclear Research, Dubna. Binding energies (masses), Q_α values and α -decay half-lives of many nuclei have been determined or estimated. Naturally, such data is accessible only for light mass SHE especially with $Z = 100 - 110$. Only few data exist for $Z = 112$ and

$Z = 114$.

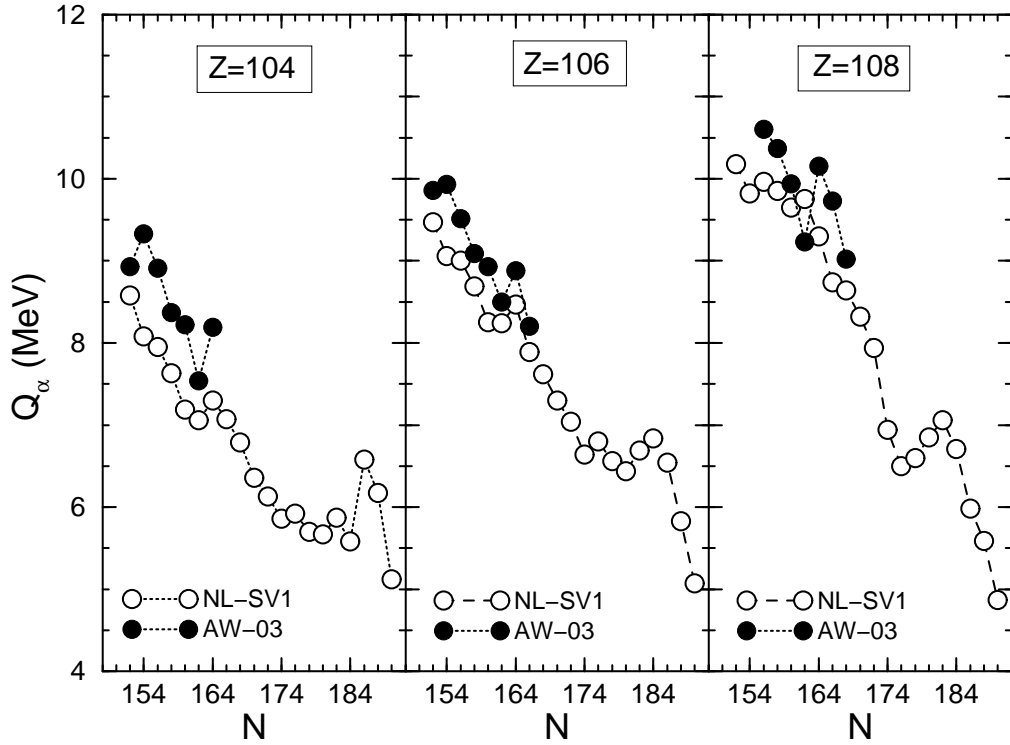


Figure 9. Q_α values obtained with NL-SV1 for the isotopic chains with $Z = 104, 106$ and 108 for the neutron numbers ranging from $N = 150 - 190$. The experimental values taken from the systematics of Audi-Wapstra [48] are shown for comparison.

We show in Figs. 9 and 10, Q_α values obtained with NL-SV1. These are compared with Q_α values taken from 2003 compilation of systematics by Audi-Wapstra [48]. As seen in Fig. 9, NL-SV1 values underestimate the empirical Q_α values for $Z = 104 - 108$ slightly. The disagreement was a bit more pronounced for $Z = 104$. For $Z = 106$ the agreement of NL-SV1 values with the data is reasonably good. For the case of $Z = 104$ and $Z = 106$, the kink in Q_α values at $N = 162$ in the experimental data is reproduced well by NL-SV1. For the chain of $Z = 108$, though NL-SV1 values are close to the experimental data, the kink at $N = 162$ in the experimental data is not reproduced by NL-SV1. This may be due to complex shell structure around $Z = 108$ than that presented by the mean field in the RMF.

In Fig. 10 the NL-SV1 values show agreement with several data points, whereas there is a discrepancy of more than 1 MeV for the data points of $N = 158$ and $N = 166$. Such differences may arise from a different evolution of shape in reality than predicted by the theory. In contrast, the NL-SV1 values show a very good agreement with experimental data for SHE chain with $Z = 112$. It may however be mentioned that for $Z = 112$ the empirical data available is limited to four data points. The number of data points available for $Z = 114$ is limited to two points only. The trend of these two

data points is represented quite well by the theoretical values, though the discrepancy for data point at $N = 174$ is little more than 1 MeV. Given the complex picture of superheavy region that evolves due to interplay between deformation and single-particle states, the theoretical description of Q_α values as seen in Figs. 9 and 10 can be considered as satisfactory.

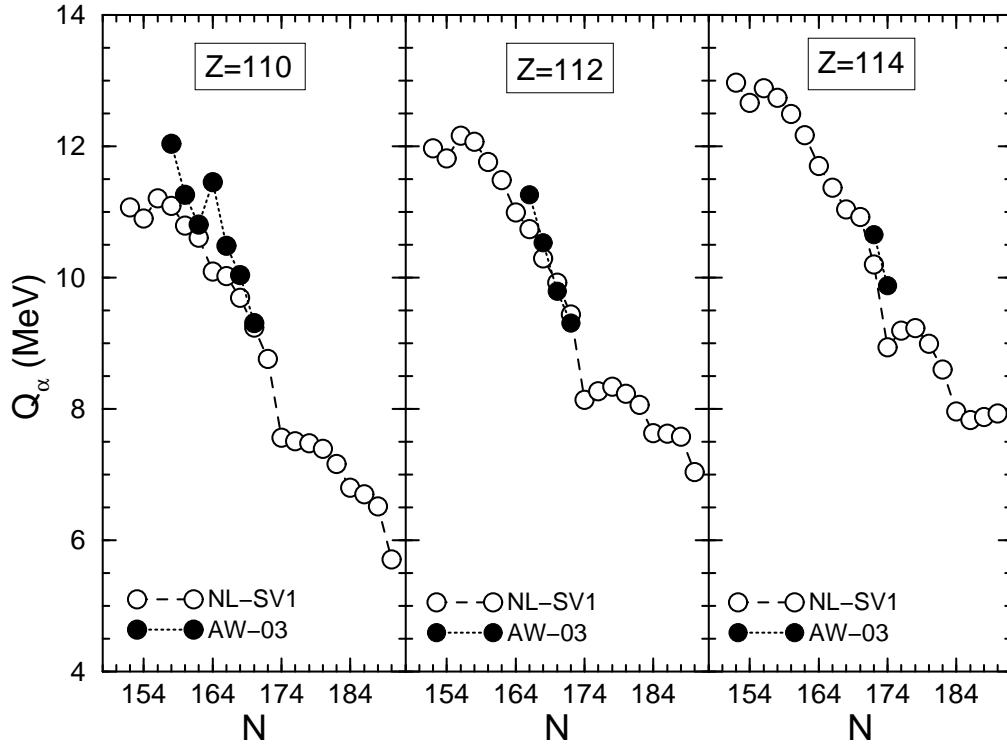


Figure 10. Q_α values obtained with NL-SV1 for the isotopic chains of $Z = 110, 112$ and 114 for the neutron numbers $N = 150 - 190$. The experimental values taken from the systematics compiled by Audi-Wapstra [48] are shown for comparison.

4.7. Alpha-decay half-lives

Using the Q_α -values, α -decay half-lives can be calculated using the phenomenological formula of Viola and Seaborg as given by,

$$\log T_\alpha = (aZ + b)Q_\alpha^{-1/2} + (cZ + d), \quad (16)$$

where Z is the atomic number of the parent nucleus and Q_α is the α -decay energy in MeV. Then, T_α is obtained in seconds. The parameters a, b, c and d have been fitted to α -decay half-lives of known nuclei over a large range. This includes new experimental data obtained in the last decade. The values of a, b, c and d have been obtained by Sobiczewski et al. [49]. The values of these parameter are $a = 1.66175$, $b = -8.5166$, $c = -0.20228$, and $d = -33.9069$.

Using the Viola and Seaborg formula of Eq. (16), we have calculated the α -decay half-lives T_α for nuclides in all the isotopic chains. The results are shown in Fig. 11. As can be seen from Eq. (16), $\log T_\alpha$ is inversely proportional to $\sqrt{Q_\alpha}$. The decreasing trend of Q_α with neutron number as shown in Fig. 8 translates into an increasing trend for $\log T_\alpha$. As seen in Fig. 11, $\log T_\alpha$ values show a rather linear increase with neutron number in the region $N = 150$ to $N = 180$ for all the isotopic chains with the exception of the heaviest SHE $Z = 116 - 120$. The latter show a linear behaviour in the curves in the neutron region $N = 150 - 170$. Above $N = 170$ the slope exhibits a further increase in the value of $\log T_\alpha$. A nearly linear increase of $\log T_\alpha$ with neutron number implies an exponential increase in T_α in going to higher neutron numbers. The half-life curve shows the highest values for the isotopic chain $Z = 102$. As the Z value of an isotopic chain increases, the half-life curves show a gradual decrease. This shows that in going to heavier SHE, nuclides become less and less unstable.

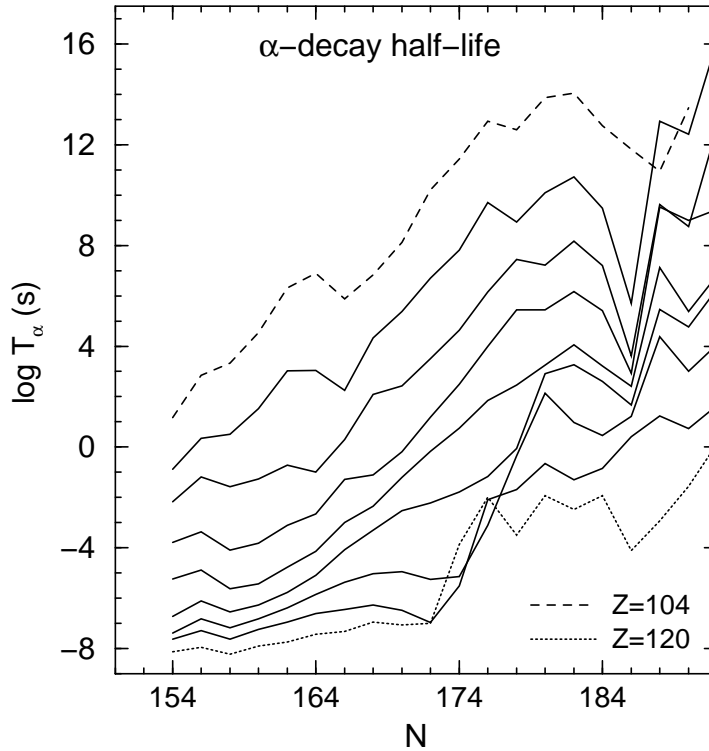


Figure 11. The $\log T_\alpha$ values for the isotopic chains with $Z = 102 - 120$ and $N = 150 - 190$ obtained with NL-SV1.

Commensurate with Q_α values in Fig. 8, one notices a few peak-like structures in half-lives at certain neutron numbers. A small peak-like structure can be seen at the neutron number $N = 154$ in nearly all the isotopic chains with the exception of the heaviest chains $Z = 118$ and $Z = 120$. The increased T_α at $N = 154$ can be understood in terms of a deformed shell gap at this neutron number. A similar behaviour (feature) has also been predicted by non-relativistic macroscopic-microscopic calculations [50].

Another minor enhancement in T_α can be seen in the vicinity of $N \sim 160 - 162$ for the isotopic chains for the lightest SHE $Z = 102 - 112$. The region of $N \sim 162$ has also been predicted to be a deformed shell [50]. A major enhancement in T_α values can be conspicuously seen near $N = 182 - 184$. A peak like structure in $\log T_\alpha$ curves can be seen near $N \sim 184$ for the isotopic chains of SHE with $Z = 102 - 112$. Apparently, $N = 182$ exhibits a higher value of T_α as compared to $N = 184$. In going to $N = 186$, there is a sudden decrease in T_α values by a few orders of magnitude especially for lighter SHE with $Z = 104 - 108$. For the chains with $Z = 110 - 112$, there is also a decrease in T_α at $N = 186$. This decrease is, however, smaller than for lighter SHE. Thus, for SHE with $Z = 102 - 114$, the region of neutron number $N = 184$ denotes a region of an enhanced stability against α -decay.

As one goes above $Z = 114$ to heavier SHE, the T_α values show a significant decrease by several orders of magnitude. Nonetheless, SHE with $Z = 116$ to $Z = 120$ still show a maximum near $N \sim 184$. This implies that even for the heavier SHE the region of $N \sim 184$ shows an enhanced stability as compared to their lighter neutron counterparts. Thus, the region with $N = 184$ would be suitable for synthesizing heavier superheavy elements. For the case of $Z = 120$ isotopic chain, there is also a peak in the T_α curve in the Fig. 11 at $N = 174$. This indicates that the combination $Z = 120$ and $N = 174$ may be suitable for synthesizing the $Z = 120$ superheavy element.

4.8. Potential energy landscapes

A potential energy landscape represents the total energy of a nucleus as a function of deformation. It reflects how a nucleus rearranges its single-particle structure under the influence of deformation. We have carried out constrained RMF calculations with the Lagrangian set NL-SV1. The quadrupole deformation β_2 is used as a constraint parameter i.e, the binding energy of a nucleus is calculated for a given deformation. The RMF calculations are carried out for each value of β_2 in the deformation plane with a small grid in β_2 .

We show in Fig. 12 the potential energy surface (PES) for a nuclide of the lighter superheavy element ${}^{278}_{104}\text{Rf}$ ($Z = 104$) with the neutron number $N = 174$. Two valleys can be seen, one in an oblate region and another in the prolate region. This picture is a clear reflection of a prolate-oblate shape co-existence whereby the two minima are nearly degenerate in energy. The actual ground state in this case is, however, prolate as shown by the slightly lower valley in the prolate region. The PES for a heavier SHE for the nuclide ${}^{300}_{116}$ ($Z = 116$) with the neutron number $N = 184$ is shown in Fig. 13. This figure illustrates a shape co-existence between a spherical and an oblate shape, as has been indicated by a blue square in Fig. 5. However, here the ground state is spherical in shape. This is consistent with $N = 184$ still retaining some magicity in going to $Z = 116$.

We show in Fig. 14 the potential energy landscape for another nuclide with $Z = 118$ and $N = 172$. It shows a clear minimum for a spherical shape ($\beta_2=0$). There is no shape

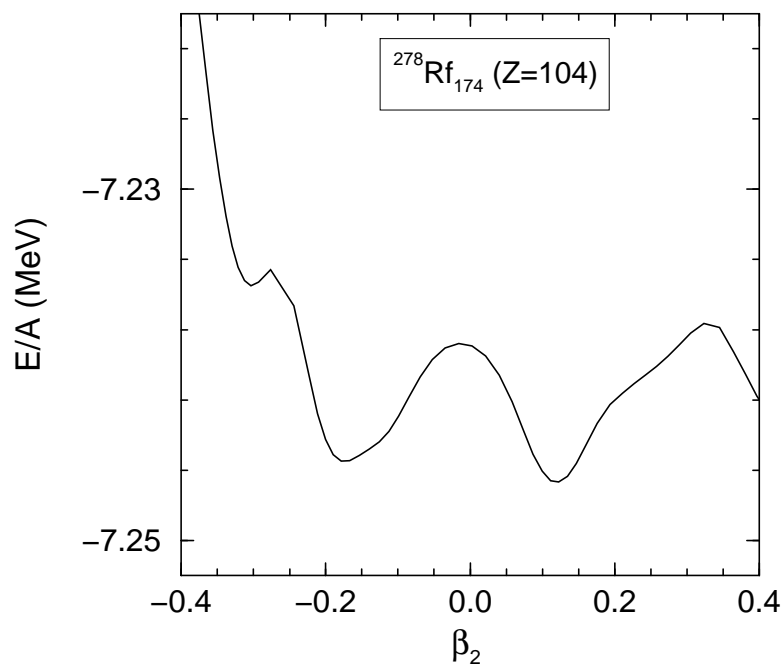


Figure 12. The potential energy landscape for $^{278}\text{Rf}_{174}$ obtained with NL-SV1.

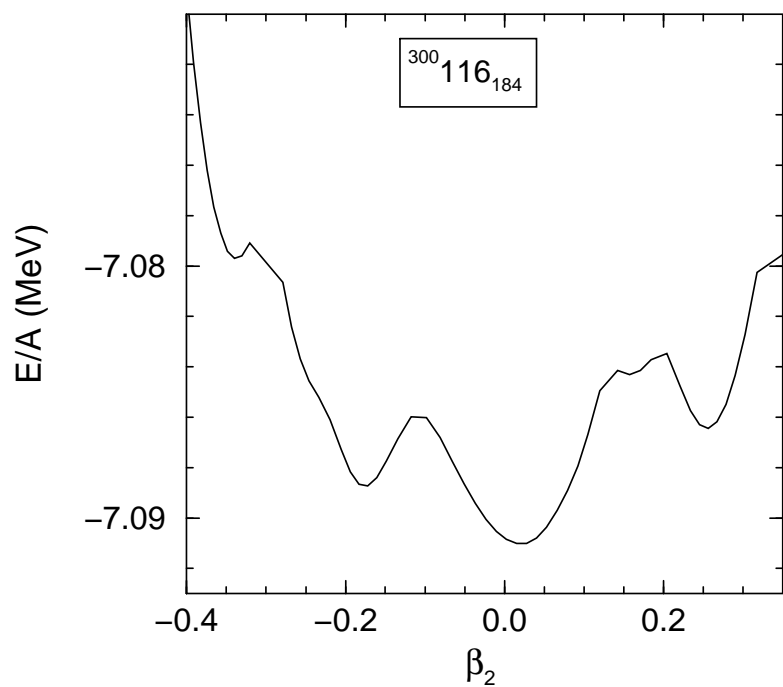


Figure 13. The potential energy landscape for $^{300}\text{116}_{184}$ obtained with NL-SV1.

co-existence with any other shape for this nucleus. The spherical shape at $N = 172$ reflects the character of a shell closure in the midst of deformed nuclei in a very heavy superheavy region. A spherical shape for $N = 172$ in the deformed region is accentuated

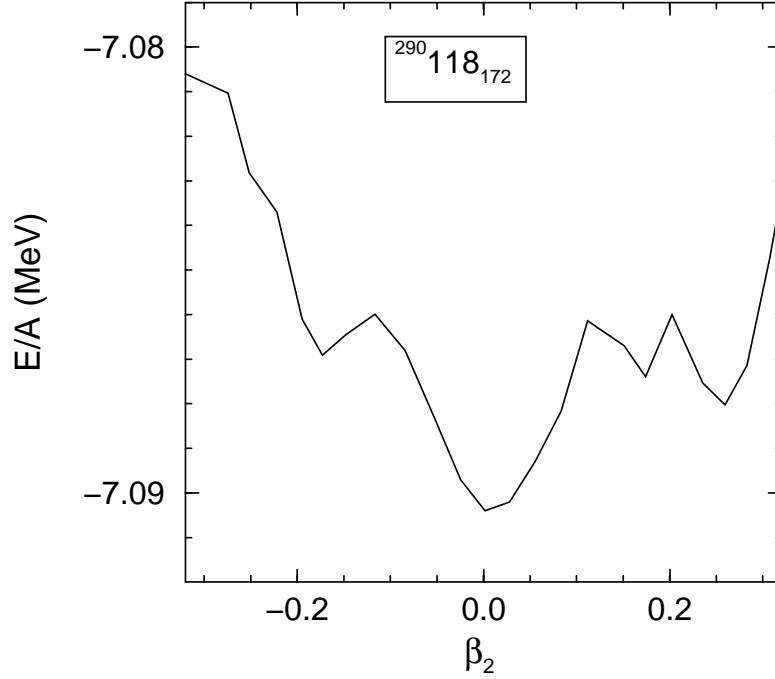


Figure 14. The potential energy landscape for $^{290}_{118}_{172}$ obtained with NL-SV1.

by the proximity of its proton number to the presumed magic number $Z = 120$.

4.9. The single-particle levels

The single-particle structure of nuclei is a good reflection of magic numbers, whereby larger shell gaps at a magic number can be seen in single-particle levels. In order to visualize some of the potential magic numbers in the region of superheavy nuclei, here we show the single-particle spectrum for a few key nuclei. As mentioned before, the neutron number $N = 172$ is perceived as akin to a magic number. We show in Fig. 15 neutron single-particle levels calculated for nuclides with $N = 172$ for SHEs with $Z = 112 - 120$. In all these nuclei the shell gaps at $N = 172$ and at $N = 184$ can be seen clearly. In these nuclei the shell gap at $N = 172$ is maintained in going from $Z = 112$ to $Z = 120$. Quantitatively, there is no change as such in the shell gap at $N = 172$ in going from $Z = 112$ to $Z = 120$. However, the gap itself is pushed down in energy in reaching $Z = 120$. Thus, the neutron number $N = 172$ would be helpful in synthesizing the superheavy elements with $Z = 118$ and $Z = 120$.

In Fig. 16 we show the neutron single-particle spectrum for nuclides with $N = 184$ for SHEs with $Z = 112 - 120$. The shell gap at $N = 184$ can be seen clearly. Thus, $N = 184$ manifests as a major magic number. This is consistent with several other theoretical predictions. In the RMF theory with NL-SV1, the shell gap at $N = 184$ shows a decrease in going from $Z = 112$ to $Z = 120$. We also see a major shell gap at $N = 198$. However, it may be of little practical importance in synthesis of superheavy

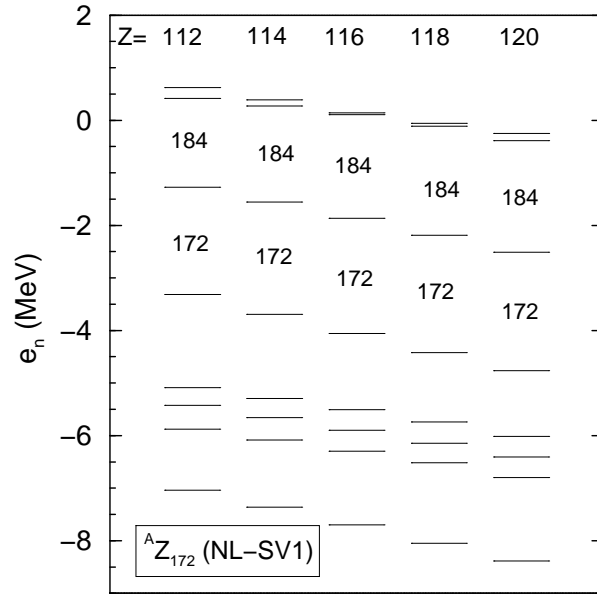


Figure 15. The neutron single-particle levels for $N = 172$ isotones for $Z = 112, 114, 116, 118, 120$ with NL-SV1.

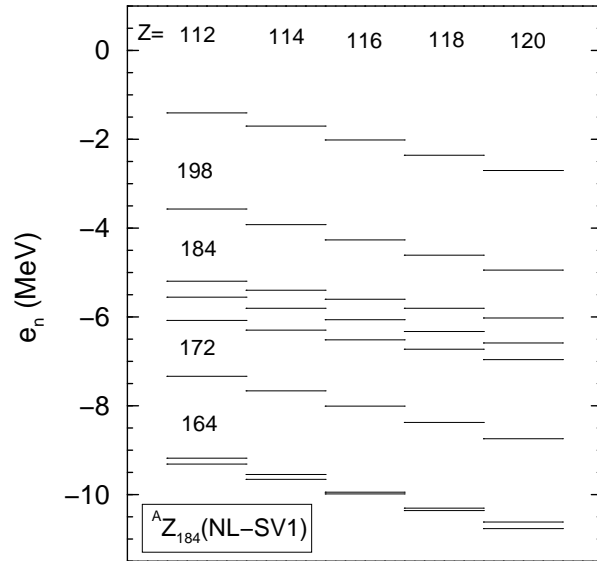


Figure 16. The neutron single-particle energy levels for $Z = 112, 114, 116, 118, 120$ and $N = 184$ with NL-SV1.

elements due to very large number of neutrons involved.

In order to visualize the single-particle structure of SHE $Z = 120$, we show in Fig. 17, the proton single-particle levels obtained with NL-SV1 for nuclides with $N = 172, N = 184$ and $N = 198$. The nuclide with $Z = 120$ and $N = 172$ is very close to being unbound. The proton shell gap at $Z = 120$ can be seen for $N = 172$, though it couples to continuum. From a practical point of view, the nuclide with $Z = 120$ and $N = 172$, which shows the character of a doubly magic nucleus can be useful in

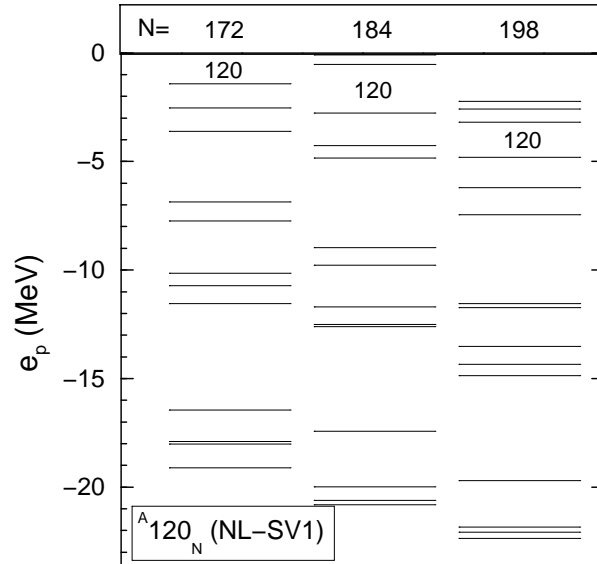


Figure 17. The proton single-particle levels for the isotopes of $Z = 120$ with $N = 172$, 184 and 198 using NL-SV1.

synthesizing SHE with $Z = 118$ and $Z = 120$. The combination $Z = 120$ and $N = 184$ also comes out as a doubly magic configuration. It may be possibly of use in synthesizing the heaviest superheavy nuclei.

5. Summary and Conclusions

We have studied the structure of superheavy nuclei within the framework of the relativistic mean-field theory. The region of superheavy elements from $Z = 102$ to $Z = 120$ has been explored. The isotopic chains of the superheavy elements encompassing the neutron number from $N = 150$ to $N = 190$ have been investigated. The Lagrangian model NL-SV1 with the inclusion of the vector self-coupling of the ω -meson has been employed.

RMF calculations for a large number of nuclides in the isotopic chains of superheavy elements have been performed by taking an axially symmetric deformed configuration. The binding energies, deformation properties and single-particle levels have been obtained from RMF+BCS minimizations. Nuclides in general are found to possess a moderate oblate or a prolate deformation. On the other hand, nuclei in the vicinity of the neutron number $N = 184$ display a spherical shape. Display of a spherical shape for all the isotopic chains indicates an inclination of $N = 184$ being toward a potential magicity.

It is shown that nuclei in the region of superheavy elements exhibit the phenomenon of shape co-existence. A large number of nuclei much below $N = 184$ exhibit a shape co-existence between a prolate and an oblate shape. This is specially the case for the isotopic chains from $Z = 102$ to $Z = 114$. Some isotopic chains exhibit a shape-

coexistence between a spherical and an oblate shape especially those in the vicinity of $N = 184$. The shape-coexistence in nuclei is demonstrated by the potential energy landscapes obtained for a few nuclei.

The Q_α values and the corresponding α -decay half-lives were obtained using the ground-state binding energies. The α -decay half-lives T_α demonstrate clearly that in the vicinity of $N = 184$ nuclides have a significantly larger T_α as compared to their neighbours. This is again a strong indicator of the magicity of the neutron number $N = 184$.

Two-neutron separation energies of nuclides were calculated using the results with NL-SV1. The S_{2n} values exhibit a small kink near $N = 160$ and $N = 172$. This suggests that the neutron number $N = 160$ and $N = 172$ have a larger shell gap than their neighbours. In comparison, a strong kink in S_{2n} values at $N = 184$ is a clearest indication of a major shell gap at $N = 184$.

The single-particle levels obtained with the Lagrangian model NL-SV1 show that there exist shell gaps at neutron numbers $N = 172$ and $N = 184$. Whilst $N = 172$ can not be construed as a major magic number as displayed by a mild kink in S_{2n} values, the neutron number $N = 184$ does behave as a major magic number in the neutron-rich region. Evidently, the magicity of $N = 184$ is demonstrated succinctly by a large shell gap at $N = 184$ seen in the single-particle levels. This picture of the magicity of $N=184$ in the RMF theory is consistent with the predictions in the density-dependent Skyrme Hartree-Fock approach and also with the previous studies performed within the RMF theory using the conventional model of the nonlinear scalar self-couplings. Thus, our study with the Lagrangian model NL-SV1 with the vector self-coupling of ω meson reinforces the magic character of the neutron number $N = 184$. Albeit, a decrease in the shell gap at $N = 184$ in going towards $Z = 120$ implies a weakening of the shell strength in approaching the extreme end of the periodic table.

Whilst a combination of $N = 184$ in conjunction with Z in the vicinity of 120 produces nuclei which have impractically large number of neutrons, the combination of the neutron number $N = 172$ and $Z = 120$ does lie within the domain of feasibility. Our study shows that this combination is suggestive of a double magicity. Thus, synthesis of superheavy elements heavier than $Z = 116$ with neutron number close to $N = 172$ should be susceptible to an extra stability rendered by the apparent magic nature of $Z = 120$ and $N = 172$.

6. Acknowledgments

This work is supported by the Graduate Research Project Y01/05 of the Research Administration, Kuwait University. Useful discussions with Professor G. M \ddot{u} nzenberg are thankfully acknowledged.

References

- [1] M \ddot{u} nzenberg G 1988 *Rep. Prog. Phys.* **51** 57
- [2] Hofmann S and M \ddot{u} nzenberg G 2000 *Rev. Mod. Phys.* **72** 733
- [3] Hofmann S, Ninov V, Hessberger F P, Armbruster P, Folger H, M \ddot{u} nzenberg G, Sch \ddot{o} tt H J, Popeko S G, Yeremin A V Saro, S Janik R, and Leino M 1996 *Z. Phys.* **A354** 229
- [4] Hofmann S, Hessberger F P, Ackermann D, M \ddot{u} nzenberg G, Antalic S, Cagarda P, Kindle, B, Kojuharova J, Leino M, Lommel B, Mann R, Popeko A G, Reshitko S, Saro S, Uusitalo J and Jeremin A V 2002 *Eur. Phys. J.* **A14** 147
- [5] Ginter T N, Gregorich K E, Loveland W Lee, D M Kirbach, U W, Sudowe R, Folden III C W, Patin J B, Seward N, Wilk P A, Zielinski P M, Aleklett K, Eichler R, Nitsche H and Hofmann D C 2003 *Phys. Rev. C* **67** 064609
- [6] Oganessian Yu Ts, Utyonkov V K, Lobanov Yu A, Abdullin F Sh, Polyakov A N, Shirokovski I V, Tsyganov Yu S, Gulbekian G G, Bogomolov S L, Gikal B N, Mezentsev A N, Iliev S, Subbotin, V G, Sukhov, A M, Buklanov, G V, Subotic, K, Itkis, M G, Moody, K J, Wild, J F, Stoyer, N J, Stoyer, M A, and Lougheed R W 1999 *Phys. Rev. Lett.* **83** 3144
- [7] Oganessian Yu Ts, Utyonkov VK, Lobanov, YuV, Abdullin, F Sh, Polyakov, A N, Shirokovski, I V, Tsyganov, Yu S, Gulbekian, G.G., Bogomolov, S.L., Gikal, B.N., Mezentsev, A.N., Iliev, S, Subbotin, V G, Sukhov, A M, Ivanov, O V, Buklanov, G V, Subotic, K, Itkis, M G, Moody, K J, Wild, J F, Stoyer, N J, Stoyer, M A, and Lougheed, R W 2000 *Phys. Rev. C* **6** (R) 041604
- [8] Oganessian, Yu Ts, Utyokoy, V K, Lobanov, Yu V Abdullin, F Sh, Polyakov, A N, Shirokovsky, I V, Tsyganov, Yu S, Gulbekian, G G, Bogomolov, S L, Gikal, B N, Mezentsev, A N, Iliev, S, Subbotin, V G, Sukhov, A M , Ivanov, O V, Buklanov, G V, Subotic, K, Itkis, M G, Moody, K J, Wild, J F, Stoyer, N J, Stoyer, M A, Lougheed, R W, Laue, C A , Karelin, Ye E and Tatarinov, A N 2000 *Phys. Rev. C* **63** (R) 011301
- [9] Oganessian, Yu Ts Utyonkov, V K , Lobanov, Yu A, Abdullin, F Sh Polyakov, A N, Shirokovski, I V, Tsyganov, Yu S, Gulbekian, G G, Bogomolov, S L, Gikal, B N, Mezentsev, A N, Iliev, S, Subbotin, V G, Sukhov, A M, Voinov, A A, Buklanov, G V, Subotic, K, Zagrebaev, V I, Itkis, M G, Patin, J B, Moody, K J, Wild, J F, Stoyer, M A, Stoyer, N J, Shaughnessy, D A, Kennally, J M and Lougheed, R W 2004 *Phys. Rev. C* **69** 054607
- [10] Ogasessian, Yu Ts, Utyokoy, V K, Lobanov, Yu V, Abdullin, F Sh, Polyakov, A N, Shirokovsky, I V, Tsyganov, Yu S, Gulbekian, G G, Bogomolov, S L, Mezentsev, A N, Iliev, S, Subbotin, V G, Sukhov, A M, Voinov, A A, Buklanov, G V, Subotic, K, Zagrabaev, V I, Itkis, M G, Patin, J B, Moody, K J, Wild, J F, Stoyer, M A, Stoyer, N J, Shaughnesy, D A, Kenneally, J M, and Lougheed, R W 2004 *Phys. Rev. C* **69** (R) 021601
- [11] M \ddot{o} ller, P, Nix, J R, Myers, W D, and Swiatecki, W J 1995 *At. Data Nucl. Data Tables* **59** 185
- [12] Cwiok, S, Pashkevich, V, Dudek, J, and Nazarewicz, W 1983 *Nucl. Phys. A* **410** 254
- [13] Cwiok, S, Dobaczewski, J, Heenen, P H, Magierski, P, and Nazarewicz, W 1996 *Nucl. Phys.* **A611** 211
- [14] B \ddot{u} rvenich, T, Bender, M, Maruhn, J A, and Reinhard, P G 2004 *Phys. Rev. C* **69** 14307
- [15] Rutz, K, Bender, M, B \ddot{u} rvenich, T, Schilling, T, Reinhard, P G, Maruhn, J A, and Greiner, W 1997 *Phys. Rev. C* **56** 238
- [16] Bender, M, Rutz, K, Reinhard, P G, Maruhn, J A, and Greiner, W 1999 *Phys. Rev. C* **60** 034304
- [17] Bender, M, Nazarewicz, W, and Reinhard, P G 2001 *Phys. Lett. B* **515** 42
- [18] Reinhard, P G, Bender, M, and Maruhn, J A 2002 *Comments on Mod. Phys.* **2** A177
- [19] Sobiczewski, A, Muntian, I, and Patyk, Z 2001 *Phys. Rev. C* **63** 034306
- [20] Muntian, I and and Sobiczewski, A 2004 *Phys. Lett. B* **586** 254
- [21] Muntian, I, Patyk, Z, and Sobiczewski, A 2001 *Acta. Phys. Pol. B* **32** 691
- [22] Muntian, I, Hoffman, S, Patyk, Z, and Sobiczewski, A 2003 *Acta. Phys. Pol. B* **34** 2073
- [23] Muntian, I, Patyk, Z, and Sobiczewski, A 2003 *Phys. At. Nuclei* **66** 1015
- [24] Strutinsky, V M 1967 *Nucl. Phys.* **A95** 420
- [25] Strutinsky, V M 1968 *Nucl. Phys.* **A122** 1

- [26] Lalazissis, G A, Sharma, M M, Ring, P, and Gambhir, Y K 1996 *Nucl. Phys. A* **608** 202
- [27] Sharma, M M, Nagarajan, M A and Ring, P 1993 *Phys. Lett. B* **312** 377
- [28] Kruppa, A T, Bender, M, Nazarewicz, W, Reinhard, P G, Vertse, T and Cwiok, S 2004 *Phys. Rev. C* **61** 034313
- [29] Sharma, M M, Lalazissis, G A, König, J and Ring, P 1995 *Phys. Rev. Lett.* **74** 3744
- [30] Reinhard P G and Flocard H 1995 *Nucl. Phys. A* **584** 467
- [31] Cwiok S, Heenen P H and Nazarewicz W 2005 *Nature* **433** 705
- [32] Hofmann S, Ninov V, Hessberger F P, Ambruster P, Folger H, Münzenberg G, Schött H J, Popeko A.G, Yeremin AV, Andreyev A N, Saro S, Janik R and Leino M 1995 *Z. Phys. A* **350** 277
- [33] Hofmann S, Ninov V, Hessberger F P, Ambruster P, Folger H, Münzenberg G, Schött H J, Popeko A G, Yeremin A V, Andreyev A N, Saro S, Janik R and Leino M 1995 *Z. Phys. A* **350** 281
- [34] Sharma, M M, Farhan A R and Mythili S 2000 *Phys. Rev. C* **61** 054306
- [35] Türler A et al 2003 *Eur. Phys. J. A* **17** 505
- [36] Wilk P A, Gregorich K E, Türler A, Laue C A, Eicher R, Ninov V, Adams J L, Kirbach U W, Lane M R, Lee D M, Patin J B, Shaughnessy D A, Strellis D A, Nitsche H, Hoffman D C 2000 *Phys. Rev. Lett.* **85** 2697
- [37] Gambhir Y K, Bhagwat A and Gupta M 2005 *Phys. Rev. C* **71** 037301
- [38] Zhang W, Meng J, Zhang S Q, Geng L S and Toki H 2005 *Nucl. Phys. A* **753** 106
- [39] Sharma M M, Farhan A R and Münzenberg G 2005 *Phys. Rev. C* **71** 054310
- [40] Serot B D and Walecka J D 1986 *Adv. Nucl. Phys.* **16** 1
- [41] Sharma M M, Lalazissis G A Ring P 1993 *Phys. Lett. B* **317** 9
- [42] Boguta J and Bodmer A R 1977 *Nucl. Phys. A* **292** 413
- [43] Gambhir YK, Ring P and Thimet A 1990 *Ann. Phys. (N.Y.)* **198** 132
- [44] Bodmer A R 1991 *Nucl. Phys. A* **526** 703
- [45] Sugahara Y and Toki H 1994 *Nucl. Phys. A* **579** 557
- [46] Möller P and Nix J R 1992 *Nucl. Phys. A* **536** 22
- [47] Aboussir Y, Pearson J M, Dutta A K and Tondeur F 1995 *At. Data Nucl. Data Tables* **61** 127
- [48] Audi G, Wapstra A H and Thibault C 2003 *Nucl. Phys. A* **729** 129
- [49] Sobiczewski A, Patyk Z and Cwiok S 1989 *Phys. Lett. B* **224** 1
- [50] Möller P and Nix J R 1994 *J. Phys. G* **20** 1681